A Data-Driven Spatio-Temporal Speed Prediction Framework for Energy Management of Connected Vehicles

Mohammad Reza Amini, Qiuhao Hu, Ashley Wiese, Ilya Kolmanovsky, *Fellow, IEEE*, Julia Buckland Seeds, and Jing Sun, *Fellow, IEEE*

***Abstract*— We present an integrated spatio-temporal framework for multi-range traction power and speed prediction for connected vehicles (CVs). It combines data-driven and model-based strategies to enable CVs energy efficiency optimization. The proposed framework focuses on urban arterial corridors with signalized intersections, and leverages the historical and real-time data collected from CVs and infrastructure to predict location-specific traction loads (e.g. acceleration at intersections), and augment them with time-specific speed profiles (e.g., stop duration at intersections). A Bayesian network is developed to provide a long-term load prediction informed by probabilistic analysis of historical traffic data at intersections and between intersections. Moreover, a shockwave profile model is adopted for modeling the queuing process at intersections by leveraging vehicle-to-infrastructure (V2I) communications, providing a short-range prediction of the vehicle speed with an enhanced accuracy. The benefits of the proposed load prediction framework are demonstrated for energy management of connected hybrid electric vehicles (C-HEVs). By incorporating the predicted loads into a multi-horizon model predictive controller (MPC), integrated power and thermal management of light-duty C-HEVs is enabled over real-world driving cycles, demonstrating a near globally-optimal fuel consumption over the entire trip with a <1% deviation from dynamic programming (DP) results.**

***Index Terms*— Spatio-temporal speed prediction, model predictive control, connected vehicles.**

NOMENCLATURE

C_{bat}	Battery capacity, $[A.h]$.
C_{eng}	Engine specific heat capacity, $[J/kg.^oC]$.
M_{eng}	Equivalent thermal mass, $[kg]$.
$\dot{m}_{fuel}$	Fuel consumption rate, $[kg/sec]$.
$\dot{m}_{fuel,nom}$	Nominal fuel consumption rate, $[kg/sec]$.
P_{bat}	Battery power, $[W]$.
P_{bat}^{aux}	Battery power for auxiliary systems, $[W]$.
P_{bat}^{trac}	Battery Power for traction, $[W]$.
P_{eng}	Engine power, $[W]$.
P_{trac}	Traction power, $[W]$.
$\dot{Q}_{air}$	Heat rate rejected by air convection, $[W]$.
$\dot{Q}_{exh}$	Heat rate rejected in the exhaust, $[W]$.
$\dot{Q}_{fuel}$	Heat rate released in combustion, $[W]$.
$\dot{Q}_{heat}$	Heat rate exchanged for cabin heating, $[W]$.
SOC	Battery state-of-charge, $[-]$.
R_{int}	Battery internal resistance, $[\Omega]$.
T_{cl}	Engine coolant temperature, $[^oC]$.
Δt	Sampling time, $[s]$.
U_{oc}	Battery open circuit voltage, $[V]$.

ACRONYMS

BSFC	Brake specific fuel consumption.
BN	Bayesian Network.
CV	Connected vehicle.
C-HEV	Connected HEV.
DP	Dynamic Programming.
EMS	Energy management strategy.
HEV/EV	Hybrid electric vehicle/electric vehicle.
HVAC	Ventilation and air conditioning.
iPTM	Integrated power and thermal management.
MPC	Model predictive control.
MH-MPC	Multi-horizon model predictive control.
SPM	Shockwave profile model.
V2V/I	Vehicle-to-vehicle/infrastructure.

I. INTRODUCTION

FUTURE vehicle speed prediction can be exploited for a preview of traction power demand and some of the thermal loads (e.g., electric battery heat load) needed by energy management systems (EMS) of conventional and electrified vehicles [1], [2], [3], [4]. The prediction of traction power demand and thermal loads for vehicles operating in highly random and uncertain traffic environments, however, has often been the missing piece of information for executing optimization-based EMS. With the emergence of connected vehicles (CVs), new opportunities have been opening up for enhanced situational awareness [5], [6] through onboard sensing and data exchanges with surrounding vehicles and infrastructures.

Manuscript received 18 August 2021; revised 18 February 2022 and 21 July 2022; accepted 13 October 2022. This work was supported in part by the University of Michigan through the United States Department of Energy (DOE), Advanced Research Projects Agency-Energy (ARPA-E) NEXTCAR Program, under Award DE-AR0000797. The Associate Editor for this article was D. Wu. *(Corresponding author: Mohammad Reza Amini.)*

Mohammad Reza Amini, Qiuhao Hu, and Jing Sun are with the Department of Naval Architecture and Marine Engineering, University of Michigan, Ann Arbor, MI 48109 USA (e-mail: mamini@umich.edu; qhhu@umich.edu; jingsun@umich.edu).

Ashley Wiese and Julia Buckland Seeds are with Ford Motor Company, Dearborn, MI 48124 USA (e-mail: awiese@ford.com; jbucklan@ford.com).

Ilya Kolmanovsky is with the Department of Aerospace Engineering, University of Michigan, Ann Arbor, MI 48109 USA (e-mail: ilya@umich.edu).

Digital Object Identifier 10.1109/TITS.2022.3215073

Many CV-related technologies, such as eco-driving [1], platooning [7], cooperative adaptive cruise control [6], and eco-cooling/heating [8], [9], benefit from look-ahead information beyond the range of their onboard sensors to fully capitalize their intended benefits. When assessing the energy-efficiency of CVs, this look-ahead information has often been assumed either to be known a priori for a given driving cycle or be made available over a short-range using learning-based [10], [11] or model-based techniques [12], [13], [14]. While some studies have investigated long-range vehicle speed prediction, those results have mainly focused on the average vehicle speed on highways [15], [16], over road segments [17], [18], [19] without intersections or at the city-scale traffic level [20], at a fixed location [21], or for a single private vehicle [22].

Achieving reliable speed and load predictions for CVs, especially in arterial corridors with signalized intersections, is challenging due to the (i) highly dynamic and stochastic nature of traffic, (ii) wide range of dynamic characteristics of CVs and associated systems, and (iii) non-uniform distribution of CVs and varying levels of availability of infrastructure-based sensors. In addition, the processes in CVs evolve over timescales spanning from milliseconds (e.g., onboard planning and computation), to seconds (e.g., traction power), to minutes (e.g., thermal loads), and potentially hours (e.g., battery charging) [23], [24], [25]. Hence preview information over different prediction horizons with different levels of requirements for fidelity and accuracy is needed for energy and mobility optimization.

In [26], [27], [28], and [29] we demonstrated that improved coordination of power and thermal systems of CVs can be achieved if a reasonably accurate long-range preview of vehicle speed is available to support the optimization of slow responding thermal dynamics, including the temperatures of the engine, battery, and cabin. In particular, for integrated power and thermal management (iPTM) of a fleet of connected hybrid electric vehicles (HEVs) traveling through an urban arterial corridor, it was shown that incorporating long-range look-ahead information may decrease fuel consumption by 4% on average, as compared to the case with only short-range look-ahead information [29], [30]. To achieve these improvements, a rule-based data classification method was proposed in [13] and [29] to categorize historical traffic data based on the coordination of vehicle arrival times at intersections with the traffic signal timing. Compared to more traditional approaches used for traffic flow estimation [11], [16], the data classification strategy in [13] showed improved accuracy in predicting the vehicle speed. It achieved this by capturing some of the key features of the traffic flow dynamics, including the average cruise speed between the intersections and the approximate acceleration/deceleration profiles at the downstream intersections.

While in [13] we demonstrated the potential of applying data analytics-based approaches to learn the speed and load profiles from the historical traffic data, the large variation in the temporal data causes large uncertainties in the predicted loads. For instance, while the acceleration profiles of the vehicles departing from an intersection are similar, the time-average of acceleration profiles observed in the historical data does not capture this feature since vehicles depart the intersection at different times during the same signal cycle. Some features of the traction load profiles are location-specific, and can be better represented in spatial domain. On the other hand, other features such as the average stop times at signalized intersections can be only inferred from temporal data. Hence, an integrated spatial and temporal data analysis is needed.

The extraction and exploration of spatio-temporal features of traffic networks using data-driven and machine learning methods have been studied in the literature for speed prediction over highways [15] and road segments [17], [20]. For iPTM of HEVs in arterial corridors, accurate prediction of passing/stopping at intersections, acceleration/deceleration at intersections, and the stop time at intersections [31] are critical, in addition to speed prediction within road segments. Furthermore, the speed forecast needs to be available over a relatively long range, e.g., the entire 3-4 km urban corridor, for the best iPTM efficiency and performance. The data-driven method presented herein is capable of generating long-term speed prediction over arterial corridors with signalized intersections that satisfy the above iPTM requirements.

The main contributions of this paper are as follows. Firstly, we develop a new framework for multi-range speed and load prediction to enable more efficient operation of CVs. Secondly, we study the application of the proposed speed prediction framework for iPTM of connected HEVs (C-HEVs) and demonstrate fuel-savings using extensive simulations over real-world urban driving cycles with closely-spaced signalized intersections. Our speed prediction framework can be also leveraged to enhance (i) the situational awareness of CVs in arterial corridors, (ii) eco-routing and eco-driving for CVs, and (iii) traffic signal control with prediction and coordination.

The key innovations of the proposed framework include

- The fusion of spatial-domain data with infrastructure-based temporal data to fill the information gap in the spatial-domain, and
- The augmentation of data-driven (Bayesian network-based) and shockwave profile model-based approaches to generate a long-range vehicle speed prediction.

Furthermore, they include the integration of short and long-term speed predictions with multi-horizon model predictive control (MH-MPC) for integrated power and thermal management (iPTM).

The rest of the paper is organized as follows: In Sec. II, the traffic simulation model and spatio-temporal features of traffic data are described. The data-driven spatio-temporal speed prediction framework is presented in Sec. III. The shockwave profile model for queue dynamic estimation and short-term load prediction/planning is also introduced in Sec. III. The results of applying the proposed speed prediction framework for iPTM of C-HEVs using multi-horizon model predictive controller (MH-MPC) are presented in Sec. IV. Finally, concluding remarks are summarized in Sec. V.

II. Spatio-Temporal Features of Traffic Data

In this section, we introduce the features of traffic data in temporal and spatial domains that are useful for speed and

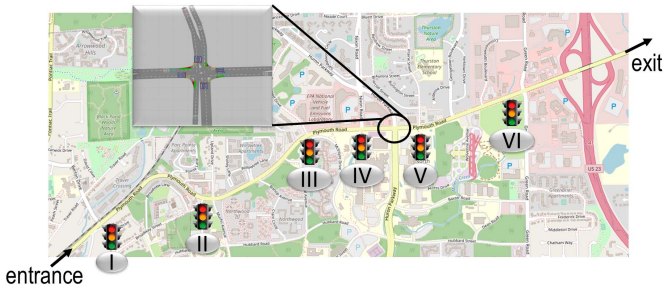

Fig. 1. The schematic of Plymouth Rd. in Ann Arbor, MI, with six intersections considered for traffic modeling, data generation, and performance evaluation.

load prediction within our use case. To generate traffic and vehicle trajectory data, a traffic simulation model of an arterial corridor is used. In the following subsections, first the utilized traffic simulation model is described. Next, the collected data from a large number of simulated vehicles traveling through the same corridor are analyzed.

A. Real-World Traffic Simulation Model and Data

A model developed in Vissim [14] is used to generate traffic data for an arterial corridor shown in Fig. 1. The corridor represents a portion of Plymouth Rd. in Ann Arbor, MI that connects Ann Arbor downtown to the US-23 Highway. The length of the corridor is around 3540 m. The corridor has two lanes in each direction and has six signalized intersections, as highlighted in Fig. 1. As described in [14], the Vissim model has been calibrated with real-world data collected during the afternoon rush hour (4:00-5:00 PM). The collected data included traffic volume, turning ratio, and traffic signal timing at each intersection. Furthermore, a queuing profile algorithm based on shockwave profile model (SPM) [12] was implemented in [14] for queue length estimation and green window[1] prediction based on the collected data from traffic signals and vehicles. The SPM will be used for short-term vehicle speed prediction and planning as will be further discussed in Sec. III-C.

B. Limitations of Temporal and Spatial Domain Data

Fig. 2 shows the data collected from the vehicles traveling along the Plymouth Rd. corridor in the time domain, plotted for different numbers of vehicles. Note that the traffic dynamics do not change during the Vissim simulation, and the signal timing and phasing policy remain fixed. When the number of aggregated vehicle trajectories is small (e.g., 10-20 vehicles), it is very hard to visually identify major traffic events and dynamics, such as passing/braking at intersections, mainly due to the lack of richness in the data. Once the number of vehicles increases above 100, some features become evident. For instance, Fig. 2 shows that the average cruise speed of the vehicles is different and becomes visible for the second half of the trip. This is expected since the speed limit of the Plymouth Rd. after the sixth intersection increases. However, when the number of aggregated trajectories is large, the average vehicle speed in the time domain does not provide much useful information for vehicle speed prediction.

The example shown in Fig. 2 highlights the trade-off between richness and variations in the traffic data. Such characteristics call for data analytics and machine learning tools to mine, extract features, and learn from traffic data. Prior to applying any data-driven strategy to such data, it is important to understand the sources of variation. To that end, and without loss of generality, we separate a set of data that belongs to vehicles that pass the first intersection of the Plymouth Rd., but stop at the second and third intersections. The speed trajectories of this set of vehicles are plotted in the time domain in Fig. 3-(a). The time-average speed for the same set of vehicles is also computed and plotted in Fig. 3-(a). It can be seen that the "average" acceleration/deceleration profiles at the second and third intersections are not representative of the actual profiles at the same locations. Fig. 3-(a) shows that the average speed in the time domain exhibits smoother acceleration/deceleration profiles, underestimating the actual loads. The primary reason for such observation is the large temporal variation of the data. According to Fig. 3-(a), while most of the vehicles accelerate and decelerate at an intersection in a similar manner, they do so at different points in time. In fact, acceleration/deceleration values at intersections appear to be primarily vehicle location-specific. To test the latter hypothesis, the temporal data in Fig. 3-(a) are plotted in Fig. 3-(b) in the spatial domain, i.e., versus distance $= t \cdot$ velocity. The average of the spatial data is also calculated and shown in Fig. 3-(b).

Fig. 3-(b) demonstrates that, firstly, the average speed inferred from the spatial data represents the acceleration/deceleration loads more accurately, compared to the average speed obtained from temporal data in Fig. 3-(a). Secondly, if the average speed obtained from the spatial data is converted back to the time domain, it still provides a much better estimation of the average speed as compared to the one obtained from the temporal data. Moreover, the location of intersections can be easily detected from the spatial data even if there is no information available about the road topology and infrastructure distribution. Despite these promising benefits, analysing the traffic data only in the spatial domain is associated with some limitations. The main drawback of spatial-domain analysis of traffic data is the loss of time-specific information, particularly, the stop periods at intersections where the vehicle locations remain unchanged. Time-specific information is, in particular, important for optimization of operation of vehicular thermal systems such as the engine or the air conditioning (HVAC) systems. The states of these thermal systems, e.g., battery and cabin temperatures, vary over time even if vehicle is stopped.

III. Spatio-Temporal Speed Prediction

To leverage both location-specific and time-specific information that are extractable from traffic data, an integrated spatio-temporal speed prediction is developed in this section. To that end, we propose to leverage data analytics and

[1]Green window is defined as the time interval during which an ego-vehicle can pass an intersection.

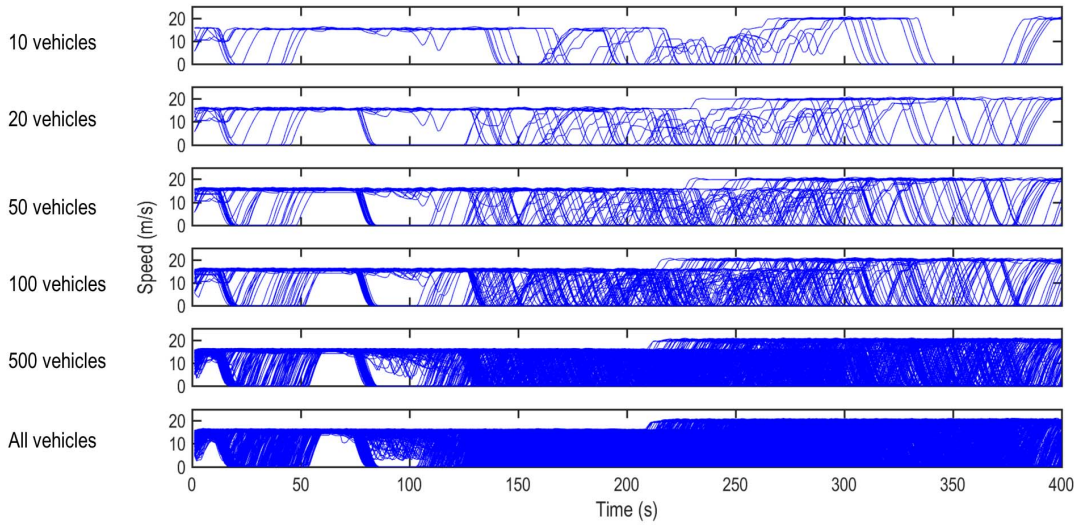

Fig. 2. The aggregated trajectories of vehicles traveling through Plymouth Rd. in the time-domain.

learning-based algorithms whose application has attracted considerable attention in recent years for transportation systems, from vehicle localization [32], [33] and traffic flow forecast [34], [35], [36] to pavement assessment [37], [38]. In particular, our objective is to exploit these data-driven techniques for historical traffic data (e.g., data shown in Fig. 2) over an arterial corridor with multiple close-spaced signalized intersections to obtain a long-term prediction of the traction power load and vehicle speed. In particular, the following features are extracted and predicted from the traffic data:

- *passing/stopping* events at intersections, which can be used to estimate the trip time, arrival time at destination, the required energy to complete the trip, and the thermal loads during stops,
- *acceleration/deceleration* profiles at signalized intersections, which can be leveraged to maximize the regenerative braking energy and enforce the hard constraint on power and thermal systems,
- *average cruise speed* between intersections, which can be capitalized on to estimate the required energy to complete the trip and the extra thermal and electrical energy that can be stored in the engine coolant and battery, respectively.

Towards this end, a data-driven method is developed first for long-term spatio-temporal prediction of vehicle speed, in which a Bayesian Network (BN) is used to classify the traffic data and generate a long-term driving scenario tree. The BN development is followed by the augmentation of time-specific information extracted from historical traffic data. Next, a model-based strategy based on the shockwave profile model (SPM) is adopted to provide a short-range temporal prediction for ego-vehicle speed based on the real-time vehicle-to-infrastructure (V2I) communications. The proposed spatio-temporal speed prediction framework is shown in Fig. 4.

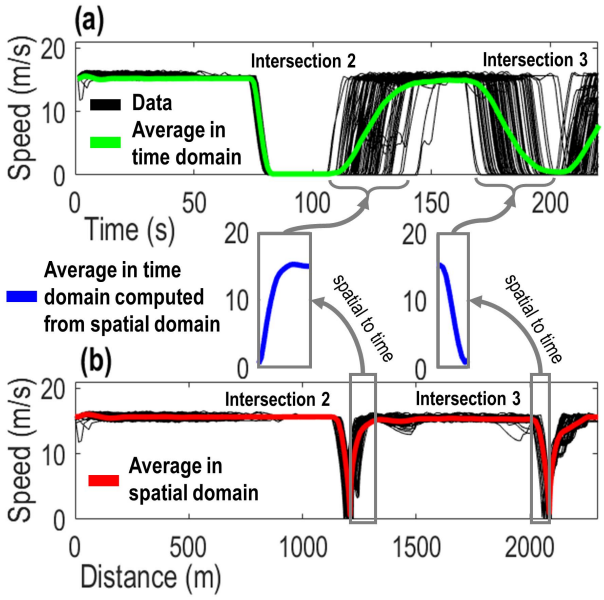

Fig. 3. Trajectories of vehicles travelling over the first three intersections of Plymouth Rd. in (a) time, and (b) spatial domains. Only the data of those vehicles that pass the first intersection, but stop at the second and third intersections are selected for better visualization purpose.

A. Bayesian Network for Data Classification

We treat passing/stopping events at intersections as stochastic variables (x) dependent on the observed events at upstream intersections. These events influence the probability distributions of the variables at downstream intersections. A Bayesian Network (BN) can take into account the causal relationship between the variables of interest and represent conditional independencies between a set of random variables [34]. Such a BN is developed offline using the historical data and can be exploited to generate a dynamic scenario tree to obtain the joint probability distribution of passing/stopping events at different intersections, based on which the "most probable" driving scenario is determined. Fig. 5 shows the concept of BN, in which the most probable driving scenario is constantly updated over time according to (i) observations obtained from the actual driving, and (ii) changes in the probability distribution of passing/stopping events as traffic evolves. In

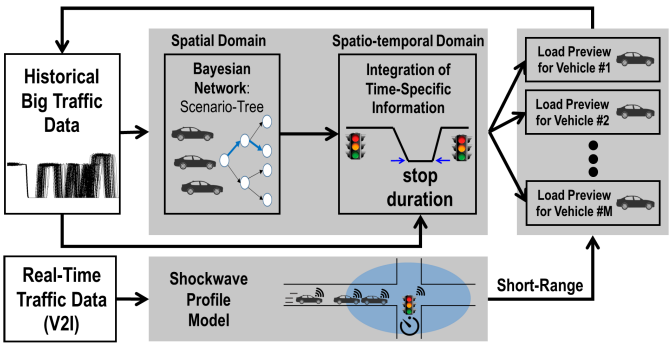

Fig. 4. The schematic of spatio-temporal load prediction framework.

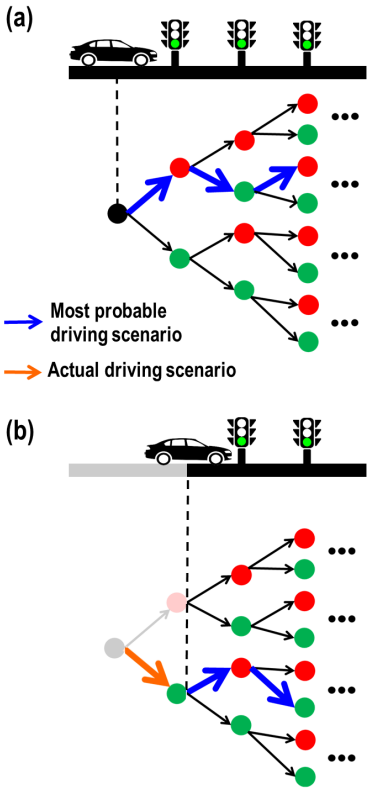

Fig. 5. The concept of BN for traffic data classification: Driving scenario tree with most probable driving scenario that is updated based on actual driving observation.

particular, while from the beginning the ego-vehicle in Fig. 5 is predicted to stop at the first intersection (Fig. 5-(a)) as the computed probability of stopping is larger than that of passing, the actual observation indicates that it passes the first intersection. Consequently, the most probable driving scenario is updated once the ego-vehicle passes the first intersection (Fig. 5-(b)).

In a BN representing an arterial corridor, an arc from intersection p to $p+1$ can be interpreted as stop/pass at intersection p followed by stop/pass at intersection $p+1$. For a corridor with H intersections, each intersection is considered as a node represented by x_k $(k = 1, \cdots, H)$, where x_k takes the values of "true" for passing and "false" for stopping. At the beginning of the trip, the joint probability distribution is calculated as [39]

$$Pr(x_1, x_2, \cdots, x_H) = \prod_{k=1}^{H} Pr(x_k | x_{\mathbf{P}_k}). \quad (1)$$

At intersection p, the joint probability distribution for the remaining trip is updated as

$$Pr(x_p, \cdots, x_H) = \prod_{k=p}^{H} Pr(x_k | x_{\mathbf{P}_k}). \quad (2)$$

Here $Pr(x_k|x_{\mathbf{P}_k})$ is the conditional probability distribution associated with intersection k and $\mathbf{P}_k$ is the set of indices labeling the upstream intersections of the k^{th} intersection [34], [40]. For instance, $Pr(x_4|x_1 = \text{True}, x_2 = \text{False}, x_3 = \text{False})$ indicates the probability of the ego-vehicle passing the fourth intersection after it has passed the first, but stopped at the second and third intersections. Given the nature of the problem, the directed arc of the BN should flow forward both in the time direction and in the traffic flow direction [34].

1) Bayesian Network Case Study: As a case study, we use the same data shown in Fig. 2 for the development and training of the BN. The speed profiles of 1478 vehicles traveling through the entire Plymouth Rd. corridor in the same direction are collected, and then 90% of these vehicle data are randomly selected for the training of the BN. Note that the total number of vehicles traveling through this corridor is larger than 1478 as some vehicles may have entered or exited the Plymouth Rd. corridor at any of the intersections shown in Fig. 1. The conditional probabilities of passing/stopping at six intersections of the Plymouth Rd. corridor are calculated by analyzing the data shown in Fig. 2, and the results are summarized in Fig. 6 as the driving scenario tree. At each intersection, the most probable driving scenario to complete the trip is determined as the branch with the highest value of the product of probabilities according to (1) and (2) and the current observation of passing/stopping event.

While in this study we utilized simulated traffic data to develop the BN and demonstrate our speed prediction approach, we envision that for real-world implementation of such a data-driven speed prediction method, traffic flow data could be continuously collected from smart infrastructure and delivered to the vehicle through any number of communication technologies, e.g., long-range radio (LoRa), fifth-generation (5G), and beyond 5G (B5G) wireless networks [41]. Additional vehicle and cellphone connectivity [11], [16] capabilities could also be leveraged if available, in accordance with appropriate consent and privacy legislation. Such data may be aggregated and analyzed in a central/cloud server, potentially even in real-time. Further study of the interplay with the data transmission infrastructure is left to continuing research.

B. Augmentation of Time-Specific Information

We next propose an approach to create a spatio-temporal prediction of the vehicle speed over a long range. The data-driven prediction in the time-domain is based on the average stop duration of vehicles at intersections, that is obtained from historical data.

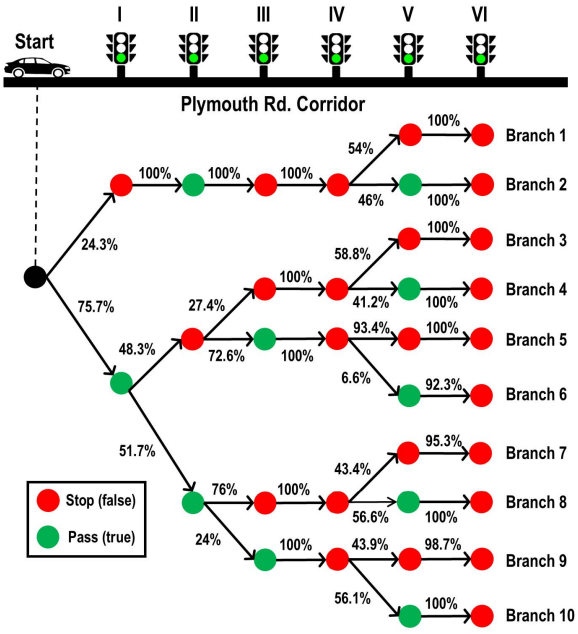

Fig. 6. The Bayesian network developed based on the historical traffic data over the Plymouth Rd. corridor.

TABLE I

THE AVERAGE, MINIMUM, AND MAXIMUM OF STOP DURATION AT EACH INTERSECTION OF THE PLYMOUTH RD. CORRIDOR

Intersection No.	Average Stop Time $[s]$	Minimum Stop Time $[s]$	Maximum Stop Time $[s]$
I	16	1	34
II	48	19	71
III	21	1	33
IV	24	0	55
V	6	0	18
VI	65	52	73

1) Case Study of Time-Specific Information: The data shown in Fig. 2 are revisited, for which the average, minimum, and maximum of stop duration at each intersection in the Plymouth Rd. corridor are calculated. The statistics are summarized in Table I. The calculated average stop duration is then fused with the speed and load predictions obtained from the driving scenario tree. Since the presence of intersections can be easily detected in the spatial domain data, augmentation of stop times is straightforward, as summarized in Fig. 7.

C. Shockwave Profile Model

For implementation in each individual ego-vehicle, the long-range speed predictions obtained from historical data need to be adapted based on the actually observed ego vehicle's current driving profile. Moreover, assuming an ego-vehicle has access to V2I data, these data can be leveraged to predict the vehicle speed with higher accuracy over a short range as compared to the prediction made based on historical traffic data. Our approach along these lines is to integrate a short-range (i.e., 10-30 s) speed preview of each vehicle

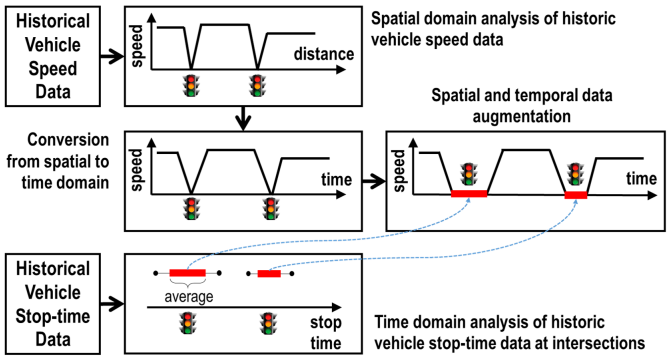

Fig. 7. The process of augmenting stop-duration information into the speed predictions informed by the spatial domain traffic data analysis.

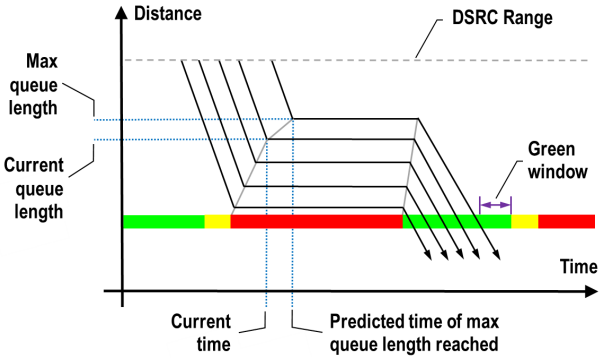

Fig. 8. SPM-based queuing profile prediction.

with the long-term look-ahead information gained from data-driven forecasts. Such integration and adaptation processes for individual vehicles are shown in Fig. 7.

For a short-range vehicle speed prediction, we exploit a model-based approach based on the SPM developed in our previous works [13], [14], which accounted for traffic signal phasing and queuing dynamics at signalized intersections and exploited real-time V2I dedicated short-range communications. The queue length is predicted based on the trajectories of CVs inferred from onboard vehicle messages and from loop-detectors installed at the infrastructure side [13], and with the consideration of vehicle acceleration/deceleration. A modified SPM model was proposed in [14] to predict the queuing dynamics and estimate the green window before an ego-vehicle arrives at an intersection. The green window prediction horizon starts from the time instant the ego-vehicle enters the communication range (i.e., 300 m) until it departs from the intersection. The concept of SPM-based queuing profile and green window predictions is shown in Fig. 8. According to Fig. 8, once the start of the green window is estimated, the speed of the ego-vehicle can be predicted to fall under one of the following driving categories based on the current signal status, current speed, distance of the ego-vehicle from the intersection, and remaining time of the signal phase: (i) slow down, (ii) speed up, (iii) cruise, or (iv) stop. Once the driving category and the approach of an ego-vehicle to an intersection are known, the short-range vehicle speed can be predicted, or optimized for eco-driving, see [14] and [13] for

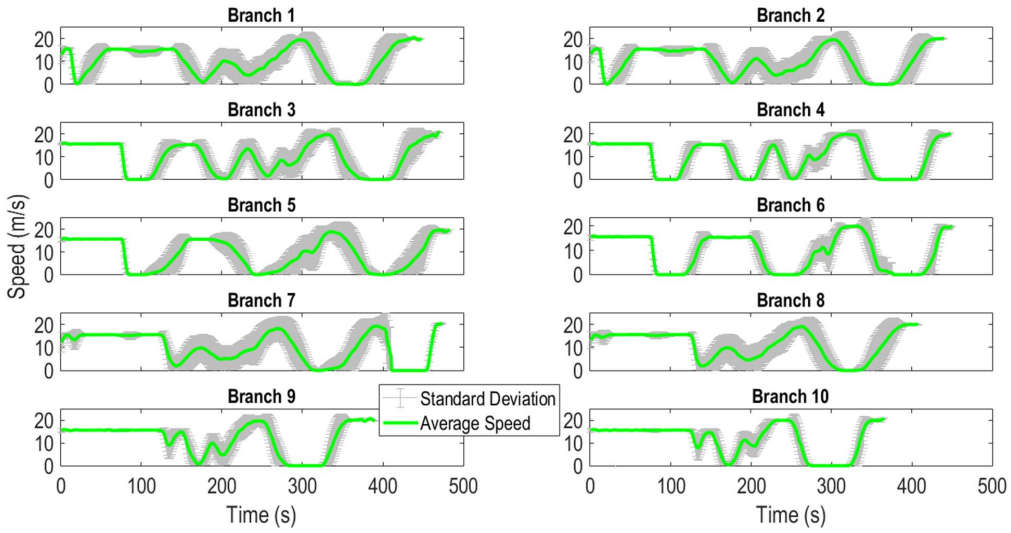

Fig. 9. The average and standard deviation of the vehicle speed data in the time domain over Plymouth Rd., classified into 10 branched using the BN.

more details, as well as for the Plymouth Rd. eco-trajectory planning case study.

Remark 1: In this paper, we assume the destination is known a priori. Moreover, for all the case studies considered in the paper, it is assumed that the destination is at the end of the corridor from which the traffic data are collected and the spatio-temporal speed prediction framework is applied to.

D. Spatio-Temporal Speed Prediction Case Study

To illustrate the proposed spatio-temporal speed prediction framework, the same traffic data of Plymouth Rd. that was shown in Fig. 2 and classified using BN are considered. Upon classification of the vehicle data into the ten branches of the BN (Fig. 6), the vehicle trajectories are aggregated for each branch. The classified data in the time domain are shown in Fig. 9, in which the mean value and standard deviation of the vehicle speed data in each branch are plotted. Compared to the raw and unclassified data in Fig. 2, Fig. 9 shows that BN-based classification of the traffic data leads to a significantly better clustering of the traffic flow and major events. Specifically, (i) passing/stopping events for all six intersections, (ii) cruising speed between intersections, and (iii) trip end times can be estimated using the developed BN. Despite the enhanced load prediction obtained through BN-based data classification in the time-domain, Fig. 9 shows that the "average" acceleration/deceleration profiles at intersections do not match the actual profiles in Fig. 2. This observation is consistent with the earlier discussion in Sec II-B on the data in Fig. 3, once again motivating to apply the BN to the historical data in the spatial domain.

Fig. 10 provides an example that compares the temporal speed predictions obtained via the BN against the spatio-temporal predictions for the same vehicle. For the spatio-temporal prediction, the same BN is applied to the traffic data in the spatial domain, then the results are converted to the time-domain and augmented with average stop times according to Table I and Fig. 4. While temporal predictions can capture the trends in the traffic flow (e.g., stop/pass, cruise speed between intersections) via the BN classification, Fig. 10 shows that the proposed spatio-temporal load prediction framework enhances the vehicle speed preview accuracy by providing a more accurate estimation of the future acceleration/deceleration profiles and stop duration at intersections. Note that, according to Table. I, the estimated average stop duration is associated with uncertainties which are reflected in the examples shown in Fig. 10.

IV. Application of Spatio-Temporal Speed Prediction for iPTM of CVs

The proposed spatio-temporal speed prediction strategy presented in Sec III enables optimization-based energy management that leverages speed (and consequently load) predictions while accounting for dynamics of power and thermal systems of CVs. To that end, in the following subsections, we first introduce the power and thermal models of an HEV that will be used to assess the benefits of the proposed speed prediction strategy on the energy use of C-HEVs. Next, we introduce an energy management strategy (EMS) based on multi-horizon model predictive control (MH-MPC) for iPTM of C-HEVs that incorporates the predicted speed as look-ahead information to perform predictive optimization.

A. Models of Power and Thermal Systems of C-HEVs

We consider a fleet of light-duty C-HEVs in this paper with a power-split powertrain configuration. For such C-HEVs, the combustion engine and electric battery are the two sources of energy that respond to traction power demand for driving the vehicle. Additionally, the battery provides power for various auxiliary loads across the vehicles, e.g., HVAC system. In this paper, we focus on C-HEV operation at cold ambient temperatures, during which heating energy needs to be provided to the cabin compartment to ensure passengers' comfort through the HVAC system. Since the combustion engine is the only source of energy for cabin heating in HEVs, the operation of

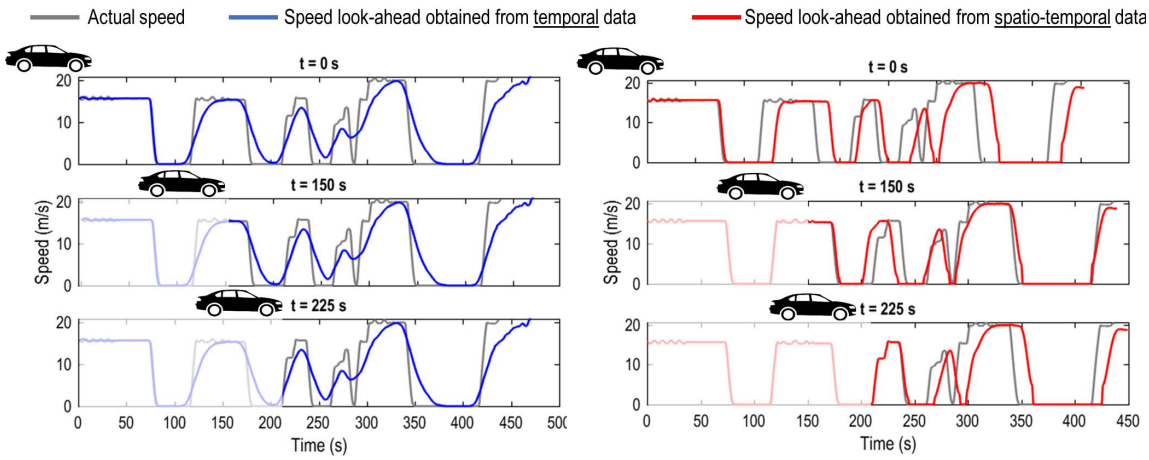

Fig. 10. The speed look-ahead information obtained from (left) temporal and (right) spatio-temporal domains data.

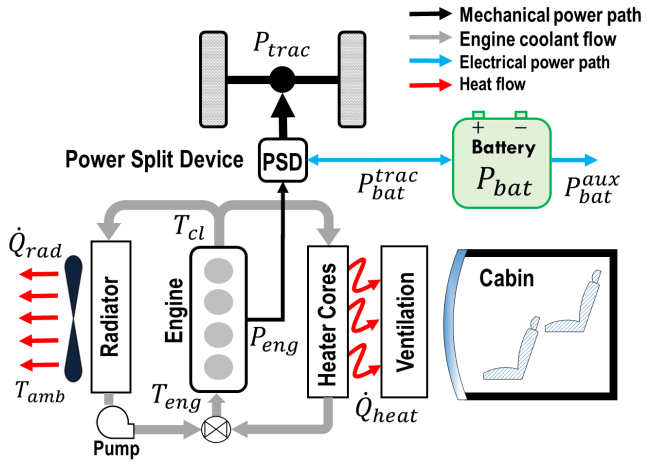

Fig. 11. Schematic of a power-split HEV with thermal and power loops.

the HVAC system demands more engine power, affecting the overall energy flow within the vehicle. The overall schematic of the power and thermal loops of an HEV is given in Fig. 11. Here, we assume the combustion engine and battery represent main sources of power, while the thermal behavior of the system is represented by engine coolant temperature.

1) Battery and Engine Power-balance Model: To meet the traction power demand (P_{trac}) for driving, the output power of battery (P_{bat}^{trac}) and engine (P_{eng}) are blended via the power-split device (PSD):

$$P_{trac} = P_{bat}^{trac} + P_{eng}. \tag{3}$$

The total battery power (P_{bat}) is

$$P_{bat} = P_{bat}^{trac} + P_{bat}^{aux}, \tag{4}$$

where P_{bat}^{aux} is the power required for the operation of auxiliary systems, including the engine and cabin thermal management systems' actuators (e.g., electric coolant pump and HVAC blower). An equivalent circuit model [42] is used to represent the battery state-of-charge (SOC) dynamics:

$$\dot{SOC}(t) = f_{SOC}(t) = \frac{U_{oc}(t) - \sqrt{U_{oc}^2 - 4R_{int}P_{bat}(t)}}{2R_{int}C_{bat}}, \tag{5}$$

with t denoting time, and C_{bat}, R_{int}, and U_{oc} being the battery capacity, internal resistance, and open-circuit voltage, respectively. See [42] and [28] for experimental validation results of the battery SOC model (5).

In (3), P_{trac} is computed according to vehicle dynamics and predicted speed. We treat P_{bat} as the decision variable to be determined by the EMS based on P_{trac}. Once P_{bat} is decided, the demanded engine power $P_{eng} = P_{trac} - P_{bat}^{trac}$ is calculated, based on which, the optimal engine operating states (engine speed (ω_e) and torque (τ_e)) are determined according to the brake-specific fuel consumption (BSFC) map. Eventually, the engine nominal fuel consumption ($\dot{m}_{f,nom}$) is obtained as

$$\dot{m}_{f,nom} = f_f(\omega_e, \tau_e), \tag{6}$$

where $f_f(\omega_e, \tau_e)$ is the nominal fuel consumption rate map. The actual fuel consumption rate ($\dot{m}_f$), however, varies as a function of engine coolant temperature (T_{cl}), degrading at low temperatures, i.e., $T_{cl} < 60^oC$ [42], [43], [44]:

$$\dot{m}_f = \alpha(T_{cl}) \cdot \dot{m}_{f,nom} \tag{7}$$

where $\alpha(T_{cl}) \geq 1$ is a multiplier reflecting the fuel consumption sensitivity to T_{cl}. These functions (BSFC map, f_f, α) are adopted from the Autonomie[2] software, also see [42] for more details.

2) Engine Coolant Temperature Model: To minimize the fuel consumption, according to (7), it is often beneficial to maintain T_{cl} above 60^oC so that $\alpha \approx 1$. To do so, the engine has to burn fuel to provide thermal energy to the coolant. Meanwhile, the cold ambient temperature and the demand for heating the cabin depletes thermal energy from the coolant, causing the engine to burn more fuel to catch up with the heat depletion from the coolant and keep its temperature above 60^oC.

[2]Autonomie® is a MATLAB®/Simulink®-based system simulation tool for vehicle energy consumption and performance analysis developed by Argonne National Laboratory (ANL) [44].

The thermal dynamics of engine coolant are modeled based on the energy balance [43]:

$$\begin{aligned}\dot{T}_{cl}(t) &= f_{T_{cl}}(t)\\ &= \frac{1}{M_{eng}C_{eng}}(\dot{Q}_f - P_{eng} - \dot{Q}_{exh} - \dot{Q}_{air} - \dot{Q}_{cabin}),\end{aligned} \tag{8}$$

with M_{eng} and C_{eng} being the equivalent thermal mass and the specific heat capacity of the engine cooling system, respectively. In (8), $\dot{Q}_f$, $\dot{Q}_{exh}$, $\dot{Q}_{air}$ and $\dot{Q}_{cabin}$, respectively, denote the heat rate released from the combustion process, exchanged through exhaust gases, dissipated by air convection, and delivered for cabin heating. In particular, $\dot{Q}_f$ is calculated as a function of the fuel consumption rate as

$$\dot{Q}_f = LHV \cdot \dot{m}_f, \tag{9}$$

where $\dot{m}_f$ is obtained from (7) and LHV is the lower heating value of the fuel (e.g., gasoline). While the cabin heating power ($\dot{Q}_{cabin}$) depends on the passenger preference, without loss of generality, a constant cabin heating power $\dot{Q}_{heat} = 1.5\ kW$ is assumed in this paper at the ambient temperature of -10^oC. For the details on the rest of the terms in (8) and model validation results, see [42], [44], and [43].

Remark 2: There are two special features of the C-HEV dynamics that are noteworthy. Firstly, there exists a strong coupling between power and thermal systems and the traction power demand. Secondly, power and thermal dynamics respond over different timescales. Accounting for such coupling makes the design of an EMS challenging, as one has to also take the timescale separation between fast power and slow thermal systems into account [27], [28]. These features motivate the use of a multi-timescale predictive optimization for energy management.

Remark 3: The multi-timescale characteristics of C-HEVs motivate the use of multi-range vehicle speed predictions. For optimization of fast HEV powertrain dynamics (e.g., engine and battery power), a relatively short-range (e.g., 10-30 s) look-ahead information may be sufficient to achieve near-optimal responses. For SOC dynamics and thermal dynamics associated with engine coolant temperature, a much longer look-ahead information is needed. We showed in our previous studies [29], [45] that an "approximate" long-range vehicle speed preview—without a detailed second-by-second vehicle speed forecast—may be leveraged for optimization of slow responding dynamics of HEVs as long as it reflects the main traffic events, e.g., acceleration and deceleration at signalized intersections, and the average cruise speed between the intersections. An ideal EMS strategy should be able to exploit both short-range and long-range look ahead information with different levels of accuracies.

B. Multi-Horizon MPC (MH-MPC) for iPTM of C-HEVs

To facilitate the design of the EMS for iPTM of C-HEVs according to the special characteristics described in Sec. IV-A, we adopt an MH-MPC framework [29], [30] to minimize the fuel consumption while enforcing the coolant temperature and battery SOC charge sustaining constraints. The MH-MPC is based on the solution to the following discrete-time optimal control problem:

$$\begin{aligned}\min_{P_{bat}(i)} \quad & \sum_{i=t}^{t+N-1} \dot{m}_f(i)\Delta t_1 + \sum_{i=t+N}^{t_{end}} \dot{m}_f(i)\Delta t_2,\\ \text{s.t.} \quad & SOC(i+1) = SOC(i) + \Delta t_j \cdot f_{SOC}(i),\ \ j \in \{1,2\}\\ & T_{cl}(i+1) = T_{cl}(i) + \Delta t_j \cdot f_{T_{cl}}(i),\ \ j \in \{1,2\}\\ & 0.4 \le SOC(i) \le 0.8,\\ & 40^oC \le T_{cl}(i) \le 90^oC,\\ & 0.99 \times SOC(0) \le SOC(t_{end}) \le SOC(0) \times 1.01,\\ & T_{cl}(0) = T_{cl,init},\quad SOC(0) = SOC_{init},\end{aligned} \tag{10}$$

where f_{SOC} and $f_{T_{cl}}$ are defined in (5) and (8), and $T_{cl,init}$ and SOC_{init} are the initial coolant temperature and battery SOC, respectively. The prediction horizon of MH-MPC covers the entire trip and is divided into two sections (i) a short receding horizon (from t to $(t+N-1)\Delta t_1$), and (ii) a long shrinking horizon (from $(t+N)\Delta t_1$ to the end of the trip t_{end}), where N is the length of the receding horizon. In (10), Δt_1 and Δt_2 are the update periods over the receding and shrinking horizons, respectively, and $j \in \{1,2\}$ is determined as follows

$$j = \begin{cases} 1, & \textbf{if}\ \ i \le t+N-1,\\ 2, & \textbf{if}\ \ i \ge t+N. \end{cases} \tag{11}$$

Among the inequality constraints of the MH-MPC in (10), the first two are incorporated to enforce the hard limits on the battery SOC and T_{cl} during the trip, while the third one is added to enforce SOC charge sustaining constraints. Note that the final SOC is allowed to deviate by $\pm$ 1% from SOC_{init} to avoid infeasibility in the solution of the MH-MPC optimization problem. It is also noted that the cost function of MH-MPC in (10) reflects the fuel consumption over the entire trip.

For solving the MH-MPC optimization problem, it is assumed that the engine operates on the curve of optimal operation points (OOP) on the BSFC map. The optimization problem (10) is solved using MPCTools package [46], which exploits the Interior Point OPTimizer (IPOPT) [47] and CasADi for numerical optimization. The MH-MPC optimization problem is solved every $\Delta t_1 = 1\ s$ and the first element of the computed control input sequence is applied to the system. Then, the receding horizon is shifted by Δt_1. The simulations are performed on a desktop computer with an Intel® E-2136@3.30 GHz processor.

Remark 4: One of the main benefits of MH-MPC is that it reduces the computing time as compared to conventional MPC [31]. To reduce the computational footprint of the MH-MPC over the long shrinking horizon, the data and prediction model incorporated over that horizon are sampled at a slower rate as compared to the short receding horizon, i.e., $\Delta t_2 > \Delta t_1$, see [29] and [30] for the assessment of the MH-MPC computational footprint. Moreover, the incorporation of a short receding horizon and a shrinking long horizon with different sampling rates in MH-MPC allows for handling multi-timescale power and thermal dynamics of an HEV.

Remark 5: For the implementation of MH-MPC on real-time controllers, similar to our previous work on hierarchical MPC [26], MH-MPC can be run in closed-loop in

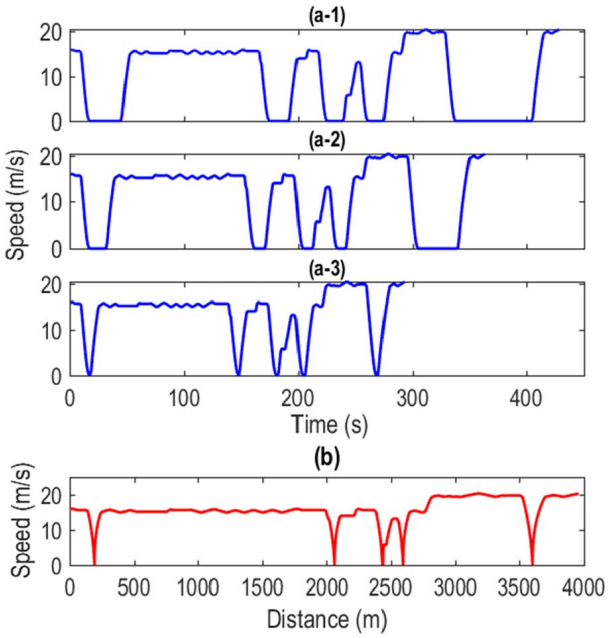

Fig. 12. (a-1,2,3) Speed profiles of three different vehicles in the time-domain, and (b) the speed profile of the same three vehicles in the spatial domain.

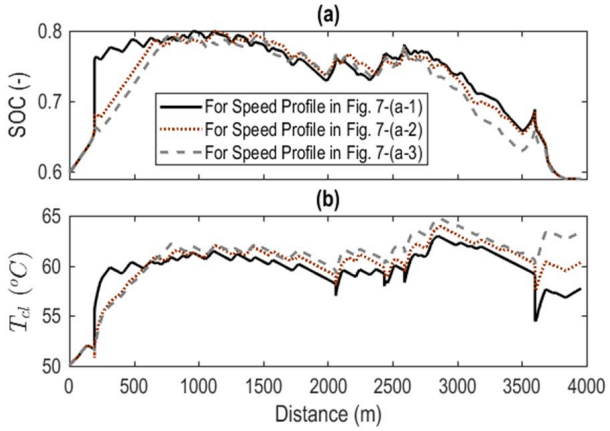

Fig. 13. The trajectories of (a) SOC and (b) T_{cl} in the spatial domain resulted from solving the iPTM strategy in the time-domain for speed profiles shown in Fig. 12-(a-1,2,3).

MATLAB/SIMULINK using C-code based on S-function, and the sequential quadratic programming [48] with Fischer-Burmeister regularized smoothed quadratic programming solver [49] to numerically solve the optimization problem. For instance, a long horizon economic and nonlinear MPC with a sampling time of 5 s and prediction horizon of 24 steps can be implemented on a Speedgoat rapid prototyping system with an Intel Celeron Core i4@2.0 GHz processor in real-time with an average computation time of 55.829 ms and a maximum computation time of up to 62 ms, see [26] for details.

1) Limitation of Implementing MPC in the Spatial Domain: While it was shown that the predictions conducted in the spatial domain result in more accurate estimation of the vehicle speed as compared to temporal predictions, performing predictive optimization in the spatial domain is not straightforward for the following reasons. Consider the following economic optimization problem that is formulated in the time-domain:

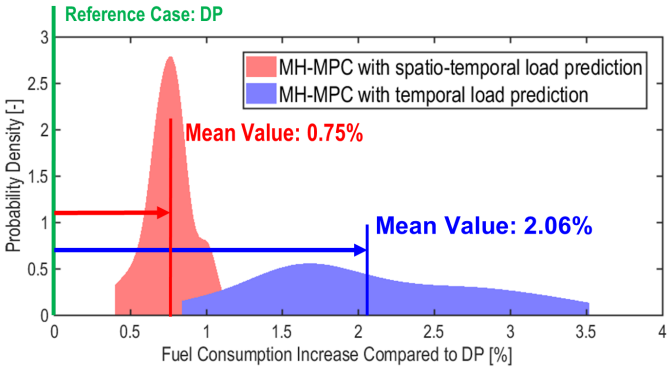

Fig. 14. The probability density function of the fuel consumption increase with MH-MPC based on the look-ahead information obtained from temporal and spatio-temporal domains. The results are compared against a reference DP case with perfect speed information. 24 vehicles from branched #3, 4, 5 of the BN are randomly selected for fuel consumption evaluation.

$$\begin{aligned} &\min_{P_{bat}(t)} \int \dot{m}_f \, dt, \\ &\text{s.t.} \quad \frac{dSOC}{dt} = f_{SOC}(t), \\ &\qquad \frac{dT_{cl}}{dt} = f_{T_{cl}}(t). \end{aligned} \tag{12}$$

To incorporate a prediction of the vehicle speed that is obtained in the spatial domain, the optimization problem in (12) can be converted to a spatial-domain optimization problem:

$$\begin{aligned} &\min_{P_{bat}(s)} \int \frac{\dot{m}_f}{v} \, ds, \\ &\text{s.t.} \quad \frac{dSOC}{ds} = \frac{f_{SOC}(t)}{v}, \\ &\qquad \frac{dT_{cl}}{ds} = \frac{f_{T_{cl}}(t)}{v}, \end{aligned} \tag{13}$$

where v and s denote vehicle speed and distance, respectively. According to (13), the main challenge of solving the optimization problem in the spatial domain is vehicle speed going to zero, which causes singularity in the cost function and state dynamics. While some studies [50], [51] have argued that solving such an optimization problem in the spatial domain alleviates high computational complexity due to nonlinearity in vehicle dynamics, most of the presented results are for scenarios that vehicle speed rarely goes to zero. However, for arterial corridors, in which vehicles often experience frequent stop-and-go behaviors, solving the MPC optimization problem in the spatial domain may not be always possible due to the singularity in the cost function and state dynamics.

Another critical issue associated with solving the MPC optimization problem in the spatial domain is the non-uniqueness of the solutions. Consider three different HEVs that drive with different speed profiles shown in Fig. 12-($a_{1,2,3}$). For these speed profiles, the MH-MPC in (10) is solved in the time domain, and the state trajectories of the optimized system are computed and then plotted in Fig. 13 in the spatial domain.

TABLE II

FUEL CONSUMPTION RESULTS FROM MH-MPC FOR IPTM WITH LOOK-AHEAD INFORMATION OBTAINED FROM TEMPORAL AND SPATIO-TEMPORAL DOMAINS FOR SAMPLE VEHICLES IN BRANCHES #3, 4, 5 OF THE BN DEVELOPED FOR PLYMOUTH RD. CORRIDOR

Vehicle No.	**DP** (Reference) (kg)	**Temporal** (kg)	**Spatio-temporal** (kg)
	Branch #3		
1	0.141	0.144 (+2.7%)	0.142 (+1.02%)
2	0.143	0.146 (+1.61%)	0.145 (+0.83%)
3	0.143	0.147 (+3.19%)	0.144 (+0.84%)
4	0.138	0.142 (+2.85%)	0.14 (+0.86%)
5	0.143	0.146 (+2.1%)	0.144 (+0.8%)
6	0.137	0.141 (+2.81%)	0.138 (+0.69%)
7	0.137	0.139 (+1.58%)	0.138 (+0.65%)
8	0.144	0.145 (+1.26%)	0.144 (+0.57%)
Average Increase		+2.26%	+0.78%
	Branch #4		
1	0.14	0.143 (+1.77%)	0.142 (+0.99%)
2	0.138	0.14 (+1.62%)	0.139 (+0.71%)
3	0.143	0.144 (+0.84%)	0.144 (+0.67%)
4	0.145	0.147 (+1.5%)	0.146 (+0.76%)
5	0.144	0.145 (+0.95%)	0.144 (+0.4%)
6	0.14	0.142 (+1.47%)	0.141 (+0.75%)
7	0.137	0.139 (+1.53%)	0.138 (+0.79%)
8	0.139	0.142 (+1.89%)	0.140 (+0.81%)
Average Increase		+1.45%	+0.73%
	Branch #5		
1	0.138	0.142 (+3.52%)	0.139 (+0.79%)
2	0.138	0.142 (+2.38%)	0.139 (+0.82%)
3	0.142	0.145 (+2.24%)	0.143 (+1.01%)
4	0.138	0.14 (+1.75%)	0.139 (+0.71%)
5	0.139	0.144 (+3.24%)	0.14 (+0.66%)
6	0.137	0.14 (+2.67%)	0.137 (+0.7%)
7	0.129	0.132 (+2.18%)	0.131 (+1.37%)
8	0.141	0.144 (+1.79%)	0.142 (+0.51%)
Average Increase		+2.47%	+0.82%

As shown in Fig. 13, the SOC and T_{cl} trajectories for these vehicles are different in the spatial domain, thus the total fuel consumption would be different. On the other hand, Fig. 12-(b) shows the speed profiles for the same vehicles in the spatial domain. Since the spatial-domain speed profile is the same for all three vehicles, the solution of an MH-MPC that is solved in the spatial-domain is also the same. The latter contradicts the results in Fig. 13.

Overall, solving MH-MPC in the time-domain is associated with fewer challenges, but the speed predictions obtained from the spatial-domain provide look-ahead information with higher accuracy. To leverage the benefits of both approaches, this study will solve the MH-MPC in the time domain, after converting spatial-domain speed predictions into the time domain.

C. Simulation Results and Discussion

This section reports the simulation results to demonstrate the benefits of the proposed spatio-temporal speed prediction strategy to enhance the energy efficiency of C-HEVs. To that end, 8 vehicles are randomly selected from each of branches #3, 4 and 5 (shown in Fig. 6), for a total of 24 vehicles. For each vehicle, the short and long-range predictions of speed profile are obtained by applying the process shown in Fig. 4. Next, the predicted speed and traction power profiles are incorporated in the MH-MPC (10). The same process is repeated for each vehicle, this time with speed predictions that are obtained from only temporal data (Fig. 9). Additionally, the results of applying offline Dynamic Programming (DP) to solve the iPTM problem are used as the benchmark for each vehicle. For DP, the exact speed profiles are assumed to be known a priori, see [42] for the details on the DP formulation and implementation.

The fuel consumption results for each vehicle are listed in Table II. For all 24 selected vehicles, Fig. 14 shows the probability density function for the fuel consumption percentage increase from MH-MPC cases as compared to DP. When MH-MPC is incorporated with speed predictions gained from temporal data, it can be seen that the average increase in the fuel consumption of C-HEVs is 2.06% when compared to DP. Such increase for the MH-MPC with spatio-temporal predictions is much smaller (0.75%), confirming the benefits of the proposed load prediction framework.

Table II shows the improved performance with the MH-MPC based on spatio-temporal predictions for individual vehicles, as well as for each branch on average. It is worth noting that the standard deviation in the MH-MPC results with spatio-temporal load prediction is also smaller than the ones resulted from the MH-MPC with temporal load predictions, see Fig. 14. The latter confirms the less inherent variability in the spatial domain, indicating the higher robustness of MH-MPC with spatio-temporal load predictions against the variations and uncertainties in the speed data.

V. SUMMARY AND CONCLUSION

We presented a speed prediction framework for energy management of connected vehicles (CVs) that leverages a data-driven spatio-temporal speed and traction load prediction strategy including a shockwave profile model. With a focus on arterial corridors with multiple signalized intersections, the goal was to maximize the use of rich traffic and connectivity data to provide a reliable look-ahead information of the future vehicle speed, as well as traction and thermal loads, to CVs to enable their energy-optimal operation. For data-driven predictions, a combination of spatial and temporal traffic data was

exploited to identify, detect, and predict location-specific (e.g., acceleration/deceleration at intersections) and time-specific (e.g., stop duration at intersections) traffic events. A Bayesian network was developed and trained based on historical traffic data to generate a dynamic and stochastic driving scenario tree, predicting the pass/stop events at signalized intersections over a relatively long prediction horizon (in this case, the entire trip). The proposed speed prediction strategy was applied to integrated power and thermal management (iPTM) of connected hybrid electric vehicles (C-HEVs) traveling through a real-world arterial corridor. A multi-horizon model predictive controller (MH-MPC) was adopted to incorporate the speed prediction and perform iPTM optimizations. Compared to an ideal benchmark scenario with perfect speed preview, the simulation results showed that a MH-MPC implemented with a time-average speed prediction leads to an increase in the fuel consumption of C-HEVs by more than 2%, on average, with a maximum deviation of 3.5%. On the other hand, the MH-MPC with spatio-temporal speed predictions showed an average increase of only 0.75% in the fuel consumption results, providing a near-globally-optimal performance.

In addition to iPTM of C-HEVs studied in this paper, vehicle speed and traffic state predictions enable a multitude of advanced CVs features, from eco-driving and eco-routing, platooning, cooperative adaptive cruise control (CACC), to more accurate ETA (estimated time of arrival) and driving range estimation for conventional and electrified vehicles, demonstrating the broader impacts of the speed prediction framework presented in this paper. At the macroscopic traffic system level, we envision that the model can be used for traffic flow modeling, analysis, and control. Our future work will focus on the sensitivity analysis of the proposed spatio-temporal speed prediction framework to the number of vehicles involved in constructing the historical traffic data, as well as expanding such framework to larger traffic networks and longer driving cycles.

ACKNOWLEDGMENT

Hao Wang and Connie Qiu from Ford Motor Company are gratefully acknowledged for their technical comments during the course of this study. Special thanks to Yiheng Feng from Purdue University and Zhen Yang from the University of Michigan for providing real-world traffic data.

REFERENCES

[1] A. Vahidi and A. Sciarretta, "Energy saving potentials of connected and automated vehicles," *Transp. Res. C, Emerg. Technol.*, vol. 95, pp. 822–843, Oct. 2018.

[2] C. Wei, T. Hofman, E. I. Caarls, and R. van Iperen, "A review of the integrated design and control of electrified vehicles," *Energies*, vol. 13, no. 20, p. 5454, Oct. 2020.

[3] J. C. C. F. Zhao and R. J. R. Gonder, "Corroborative evaluation of the real-world energy saving potentials of InfoRich eco-autonomous driving (iREAD) system," SAE Tech. Paper 2020-01-0588, 2020.

[4] P. Zhang, F. Yan, and C. Du, "A comprehensive analysis of energy management strategies for hybrid electric vehicles based on bibliometrics," *Renew. Sustain. Energy Rev.*, vol. 48, pp. 88–104, Aug. 2015.

[5] J. Rios-Torres and A. A. Malikopoulos, "A survey on the coordination of connected and automated vehicles at intersections and merging at highway on-ramps," *IEEE Trans. Intell. Transp. Syst.*, vol. 18, no. 5, pp. 1066–1077, May 2017.

[6] J. Guanetti, Y. Kim, and F. Borrelli, "Control of connected and automated vehicles: State of the art and future challenges," *Annu. Rev. Control*, vol. 45, pp. 18–40, May 2018.

[7] S. Li et al., "Dynamical modeling and distributed control of connected and automated vehicles: Challenges and opportunities," *IEEE Intell. Transp. Syst. Mag.*, vol. 9, no. 3, pp. 46–58, Fall 2017.

[8] H. Wang, M. R. Amini, Q. Hu, I. Kolmanovsky, and J. Sun, "Eco-cooling control strategy for automotive air-conditioning system: Design and experimental validation," *IEEE Trans. Control Syst. Technol.*, vol. 29, no. 6, pp. 2339–2350, Nov. 2021, doi: 10.1109/TCST.2020.3038746.

[9] M. Amini, Q. Hu, H. Wang, Y. Feng, I. Kolmanovsky, and J. Sun, "Experimental validation of eco-driving and eco-heating strategies for connected and automated HEVs," SAE Tech. Paper 2021-01-0435, 2021.

[10] S. Di Cairano, D. Bernardini, A. Bemporad, and I. V. Kolmanovsky, "Stochastic MPC with learning for driver-predictive vehicle control and its application to HEV energy management," *IEEE Trans. Control Syst. Technol.*, vol. 22, no. 3, pp. 1018–1031, May 2014.

[11] C. Sun, S. J. Moura, X. Hu, J. K. Hedrick, and F. Sun, "Dynamic traffic feedback data enabled energy management in plug-in hybrid electric vehicles," *IEEE Trans. Control Syst. Technol.*, vol. 23, no. 3, pp. 1075–1086, May 2015.

[12] X. Wu and H. X. Liu, "A shockwave profile model for traffic flow on congested urban arterials," *Transp. Res. B, Methodol.*, vol. 45, no. 10, pp. 1768–1786, 2011.

[13] M. R. Amini, Y. Feng, Z. Yang, I. Kolmanovsky, and J. Sun, "Long-term vehicle speed prediction via historical traffic data analysis for improved energy efficiency of connected electric vehicles," *Transp. Res. Rec., J. Transp. Res. Board*, vol. 2674, no. 11, pp. 17–29, Nov. 2020.

[14] Z. Yang, Y. Feng, X. Gong, D. Zhao, and J. Sun, "Eco-trajectory planning with consideration of queue along congested corridor for hybrid electric vehicles," *Transp. Res. Rec., J. Transp. Res. Board*, vol. 2673, no. 9, pp. 277–286, Sep. 2019.

[15] D. Zang, J. Ling, Z. Wei, K. Tang, and J. Cheng, "Long-term traffic speed prediction based on multiscale spatio–temporal feature learning network," *IEEE Trans. Intell. Transp. Syst.*, vol. 20, no. 10, pp. 3700–3709, Oct. 2019.

[16] J. C. Herrera, D. B. Work, R. Herring, X. J. Ban, Q. Jacobsond, and A. M. Bayen, "Evaluation of traffic data obtained via GPS-enabled mobile phones: The mobile century field experiment," *Transp. Res. C, Emerg. Technol.*, vol. 18, no. 4, pp. 568–583, Aug. 2010.

[17] Y. Kim, P. Wang, and L. Mihaylova, "Structural recurrent neural network for traffic speed prediction," in *Proc. IEEE Int. Conf. Acoust., Speech Signal Process. (ICASSP)*, Brighton, U.K., May 2019, pp. 5207–5211.

[18] B. Jiang and Y. Fei, "Vehicle speed prediction by two-level data driven models in vehicular networks," *IEEE Trans. Intell. Transp. Syst.*, vol. 18, no. 7, pp. 1793–1801, Jul. 2017.

[19] J. Park, Y. L. Murphey, R. McGee, J. G. Kristinsson, M. L. Kuang, and A. M. Phillips, "Intelligent trip modeling for the prediction of an origin–destination traveling speed profile," *IEEE Trans. Intell. Transp. Syst.*, vol. 15, no. 3, pp. 1039–1053, Jun. 2014.

[20] K. Niu, H. Zhang, C. Cheng, C. Wang, and T. Zhou, "A novel spatio–temporal model for city-scale traffic speed prediction," *IEEE Access*, vol. 7, pp. 30050–30057, 2019.

[21] X. Ma, Z. Tao, Y. Wang, H. Yu, and Y. Wang, "Long short-term memory neural network for traffic speed prediction using remote microwave sensor data," *Transp. Res. C, Emerg. Technol.*, vol. 54, pp. 187–197, May 2015.

[22] Y. Huang, Z. Xiao, D. Wang, H. Jiang, and D. Wu, "Exploring individual travel patterns across private car trajectory data," *IEEE Trans. Intell. Transp. Syst.*, vol. 21, no. 12, pp. 5036–5050, Dec. 2020.

[23] C. Atkinson, "Energy and the new mobility—How disruptive (to energy) will AVs be?" in *Proc. ARPA-E Energy Innov. Summit*, Denver, CO, USA, 2019, pp. 1–26.

[24] S. Lin et al., "The architectural implications of autonomous driving: Constraints and acceleration," in *Proc. 33rd Int. Conf. Architectural Support Program. Lang. Operating Syst.*, Williamsburg, VA, USA, 2018, pp. 751–766.

[25] A. Alleyne, "Power density as the key enabler for electrified mobility," *Polytechnica*, vol. 1, nos. 1–2, pp. 10–18, Oct. 2018.

[26] M. R. Amini, H. Wang, X. Gong, D. Liao-McPherson, I. Kolmanovsky, and J. Sun, "Cabin and battery thermal management of connected and automated HEVs for improved energy efficiency using hierarchical model predictive control," *IEEE Trans. Control Syst. Technol.*, vol. 28, no. 5, pp. 1711–1726, Sep. 2020.

[27] M. R. Amini, I. Kolmanovsky, and J. Sun, "Hierarchical MPC for robust eco-cooling of connected and automated vehicles and its application to electric vehicle battery thermal management," *IEEE Trans. Control Syst. Technol.*, vol. 29, no. 1, pp. 316–328, Jan. 2020.

[28] M. R. Amini, X. Gong, Y. Feng, H. Wang, I. Kolmanovsky, and J. Sun, "Sequential optimization of speed, thermal load, and power split in connected HEVs," in *Proc. Amer. Control Conf. (ACC)*, Philadelphia, PA, USA, Jul. 2019, pp. 4614–4620.

[29] Q. Hu et al., "Engine and aftertreatment co-optimization of connected HEVs via multi-range vehicle speed planning and prediction," SAE Tech. Paper 2020-01-0590, 2020.

[30] Q. Hu, M. R. Amini, H. Wang, I. Kolmanovsky, and J. Sun, "Integrated power and thermal management of connected HEVs via multi-horizon MPC," in *Proc. Amer. Control Conf. (ACC)*, Denver, CO, USA, Jul. 2020, pp. 3053–3058.

[31] Q. Hu, M. R. Amini, I. Kolmanovsky, J. Sun, A. Wiese, and J. B. Seeds, "Multihorizon model predictive control: An application to integrated power and thermal management of connected hybrid electric vehicles," *IEEE Trans. Control Syst. Technol.*, vol. 30, no. 3, pp. 1052–1064, May 2022, doi: 10.1109/TCST.2021.3091887.

[32] V. Havyarimana, Z. Xiao, A. Sibomana, D. Wu, and J. Bai, "A fusion framework based on sparse Gaussian–Wigner prediction for vehicle localization using GDOP of GPS satellites," *IEEE Trans. Intell. Transp. Syst.*, vol. 21, no. 2, pp. 680–689, Feb. 2020.

[33] J. Xiao, Z. Xiao, D. Wang, V. C. H. Liu, C. Zou, and D. Wu, "Vehicle trajectory interpolation based on ensemble transfer regression," *IEEE Trans. Intell. Transp. Syst.*, vol. 23, no. 7, pp. 7680–7691, Jul. 2022.

[34] S. Sun, C. Zhang, and G. Yu, "A Bayesian network approach to traffic flow forecasting," *IEEE Trans. Intell. Transp. Syst.*, vol. 7, no. 1, pp. 124–132, Mar. 2006.

[35] E. Castillo, J. M. Menéndez, and S. Sánchez-Cambronero, "Predicting traffic flow using Bayesian networks," *Transp. Res. B, Methodol.*, vol. 42, no. 5, pp. 482–509, Jun. 2008.

[36] A. Pascale and M. Nicoli, "Adaptive Bayesian network for traffic flow prediction," in *Proc. IEEE Stat. Signal Process. Workshop (SSP)*, Nice, France, Jun. 2011, pp. 177–180.

[37] S. A. Hosseini, A. Alhasan, and O. Smadi, "Use of deep learning to study modeling deterioration of pavements a case study in Iowa," *Infrastructures*, vol. 5, no. 11, p. 95, Nov. 2020.

[38] S. A. Hosseini and O. Smadi, "How prediction accuracy can affect the decision-making process in pavement management system," *Infrastructures*, vol. 6, no. 2, p. 28, Feb. 2021.

[39] T. Nielsen and F. Jensen, *Bayesian Networks and Decision Graphs*. New York, NY USA: Springer, 2009.

[40] M. Jordan, *Learning in Graphical Models*. Dordrecht, The Netherlands: Springer, 1998.

[41] X. Chen, D. W. K. Ng, W. Yu, E. G. Larsson, N. Al-Dhahir, and R. Schober, "Massive access for 5G and beyond," *IEEE J. Sel. Areas Commun.*, vol. 39, no. 3, pp. 615–637, Mar. 2021.

[42] X. Gong, H. Wang, M. Amini, I. Kolmanovsky, and J. Sun, "Integrated optimization of power split, engine thermal management, and cabin heating for hybrid electric vehicles," in *Proc. 3rd CCTA*, Hong Kong, Aug. 2019, pp. 567–572.

[43] N. Kim and A. Rousseau, "Thermal impact on the control and the efficiency of the 2010 Toyota Prius hybrid electric vehicle," *Proc. Inst. Mech. Eng., D, J. Automobile Eng.*, vol. 230, no. 1, pp. 82–92, Jan. 2016.

[44] N. Kim, A. Rousseau, D. Lee, and H. Lohse-Busch, "Thermal model development and validation for 2010 Toyota Prius," SAE Tech. Paper 2014-01-1784, 2014.

[45] M. Amini, Y. Feng, Z. Yang, I. Kolmanovsky, and J. Sun, "Long-term vehicle speed prediction via traffic data mining for improved energy efficiency of connected electric vehicles," in *Proc. TRB 99th Annu. Meeting*, Washington, DC, USA, 2020, pp. 1–13.

[46] M. Risbeck and J. Rawlings. (2016). *MPCTools: Nonlinear Model Predictive Control Tools for CasADi*. [Online]. Available: https://bitbucket.org/rawlings-group/octave-mpctools

[47] J. A. E. Andersson, J. Gillis, G. Horn, J. B. Rawlings, and M. Diehl, "CasADi: A software framework for nonlinear optimization and optimal control," *Math. Program. Comput.*, vol. 11, no. 1, pp. 1–36, Jul. 2018, doi: 10.1007/S12532-018-0139-4.

[48] M. Diehl, R. Findeisen, F. Allgöwer, H. G. Bock, and J. P. Schlöder, "Nominal stability of real-time iteration scheme for nonlinear model predictive control," *IEE Proc.-Control Theory Appl.*, vol. 152, no. 3, pp. 296–308, 2005.

[49] D. Liao-McPherson, M. Huang, and I. Kolmanovsky, "A regularized and smoothed Fischer–Burmeister method for quadratic programming with applications to model predictive control," *IEEE Trans. Autom. Control*, vol. 64, no. 7, pp. 2937–2944, Jul. 2019.

[50] S. Jacobsen et al., "Predictive cruise control behind a stationary or slow moving object," in *Proc. IEEE Intell. Vehicles Symp. (IV)*, Paris, France, Jun. 2019, pp. 2099–2105.

[51] N. K. Sharma, A. Hamednia, N. Murgovski, E. R. Gelso, and J. Sjoberg, "Optimal eco-driving of a heavy-duty vehicle behind a leading heavy-duty vehicle," *IEEE Trans. Intell. Transp. Syst.*, vol. 22, no. 12, pp. 7792–7803, Dec. 2021, doi: 10.1109/TITS.2020.3009288.